Self-Reinforcing Isotactic Polypropylene Prepared Using Crystallizable Solvents

Joonsung Yoon, Thomas J. Mccarthy, Alan J. Lesser

Department of Polymer Science and Engineering, University of Massachusetts, Amherst, Massachusetts 01003

Received 22 October 2008; accepted 23 February 2009
DOI 10.1002/app.30312
Published online 8 May 2009 in Wiley InterScience (www.interscience.wiley.com).

ABSTRACT: A new approach to reinforce and toughen isotactic polypropylene (iPP) with improved processability is evaluated. The concept involves using a crystallizable solvent that, at process temperatures melts, is miscible with the polymer thereby reducing its process viscosity. As the polymer cools, the solvent undergoes thermally induced phase separation (TIPS) to produce crystallites that increase the modulus of the solid through reinforcement and promote an increase in impact resistance by mechanisms similar to rubber-toughened materials. Tetrabromobisphenol-A (TBBPA) is introduced to iPP that forms a homogeneous mixture at elevated temperature and acts as a processing aid, but undergoes phase separation and subsequent crystallization upon cooling to form rigid particles which, in turn, acts as a toughening agent at room temperature. A phase diagram constructed with Flory-Huggins solution thermodynamics shows good agreement with the experimental results. The steady state shear viscosity decreases as TBBPA content increases for the mixtures in melt state, indicating improved processability. The decrease in viscosity enhances crystallization rate of iPP significantly, most likely due to increased diffusivity, while the structure of iPP crystals remain unchanged. Tensile tests show that as TBBPA content increases (up to 15 wt %), the yield stress decreases while elongation at break increases. © 2009 Wiley Periodicals, Inc. J Appl Polym Sci 113: 3564–3576, 2009

Key words: polypropylene; toughening; composites; particle reinforcement

INTRODUCTION

Toughening mechanisms in semicrystalline polymers has been studied extensively both experimentally and theoretically in the last few decades.[1,2] Among the many strategies to increase toughness, introducing soft rubber particles has proven most successful, despite the inevitable decrease in stiffness.[3] Many studies have shown how rubber particle size and concentration affect the increase in measured toughness. The general conclusion from these studies is that the rubber concentration should be greater than a critical value, which is a function of the particle size. Several mechanisms have been suggested to explain the toughening effect of rubbers such as multiple-crazing, damage competition, shear-yielding, microvoiding, and cavitation. However, it is generally accepted that rubber cavitation followed by either matrix shear-yielding (pseudo-ductile polymers) or crazing (brittle polymers) are major toughening mechanisms.

Cavitation should occur well before the bulk matrix failure to facilitate plastic deformation around and between particles and delocalize the fracture event. Although cavitation depends on the size of the rubber particles (larger particles cavitate before smaller ones),[4,5] matrix yielding and subsequent plastic flow depend on the particle concentration. Wu[6] combined two interdependent parameters, rubber particle size and concentration, in a single parameter, the interparticle distance. According to his argument, toughening is primarily originated by the preferential orientation of crystal planes that provide the lowest shear resistance between rubber particles. If the surface-to-surface interparticle distance is less than the critical ligament thickness, these preferentially oriented layers percolate throughout the structure and reduce plastic resistance, leading to plastic deformation. If not, the overall matrix plastic resistance is substantially elevated, which prevents plastic deformation, leading to premature brittle fracture governed by extrinsic flaws. The other requirement for this mechanism is that the particles should cavitate at the early stage of deformation to allow for unhindered stretching of the ligaments.

In contrast, rigid particles have been primarily used to improve composite stiffness and strength. Unfortunately, a notable decrease in fracture toughness is normally observed by the addition of rigid particles. This occurs primarily because the rigid particles are introduced at much higher volume fractions and treatments are done to the particles to

Correspondence to: A. J. Lesser (ajl@polysci.umass.edu).

promote high levels of adhesion. This combination results in a high composite modulus and strength since the particles become load bearing constituents. However, once the particles fail, severe strain localization occurs in the matrix under highly multiaxially constrained conditions which results in the matrix failing locally by brittle fracture rather than shear flow. The net consequence of this process usually results in reduction in material ductility and energy absorption during fracture.

However, Argon and coworkers[7,8] reported that toughness as well as stiffness can be increased simultaneously by incorporating rigid fillers under certain conditions. First, the concentration of rigid fillers must follow more closely to that of conventional rubber-toughened systems, which is usually lower than those developed to optimize strength and stiffness. Second, the interparticle distance must be below certain threshold value (a critical ligament thickness). Third, there must be low to moderate levels of adhesion between the polymer matrix and the particles. Under these conditions, Argon and coworkers surmised that the rigid particles provide some modulus enhancement at lower stress levels in contrast to conventional soft particle toughened systems. As the stress level in the material is increased, particle-matrix debonding can occur much like cavitation in rubber particles thereby relieving multiaxial stresses in the matrix and allowing many of the same toughening mechanisms observed in soft particle toughened systems to become operative in these systems. On the basis of their experimental results for semicrystalline polymers (Nylon, HDPE, and iPP) mixed with either soft particles or rigid particles, Argon and coworkers concluded that the source of the toughness is the plastic extensibility of the matrix material in the interparticle ligament and that the mechanical properties of the filler particles are of little importance for toughness.[7–12] However, it should be noted that another major drawback of this toughening approach is the detrimental effects that the filler particles have on the polymer processability. The incorporation of either soft particles or rigid particles into a polymer inevitably causes the melt viscosity to increase significantly.

In this study, we investigate a new approach to reinforce and toughen polymers. This approach involves using a crystallizable solvent to produce a composite material with improved processability, toughness, and stiffness with a single additive. The strategy involves introducing a solvent that forms a homogeneous polymer solution at the process temperatures and acts as a processing aid (i.e., plasticizer), but that undergoes phase separation and subsequent crystallization upon cooling to provide an appropriate morphology (i.e., a dispersion of crystallites) for enhanced toughness and stiffness.

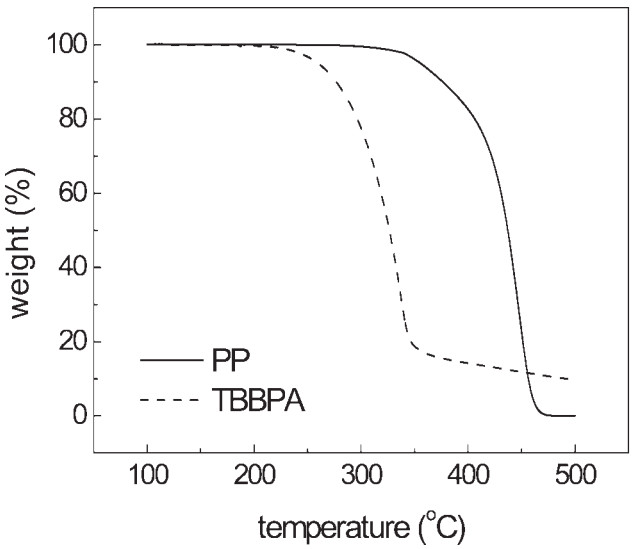

Figure 1 TGA thermogram for iPP and TBBPA measured at 10°C/min heating rate.

This article reports on initial attempts of this strategy as it is applied to iPP.[13,14]

EXPERIMENTAL

Materials

Tetrabromobisphenol-A (TBBPA) was provided by Grace Chemical (Columbia, MD) and used without further purification. Low molecular weight, high-flow isotactic polypropylene (iPP) was provided by Exxon Mobil (Houston, TX) and used as received. Molar mass of iPP was determined by a gel permeation chromatography (GPC, PL-GPC 220) at 145°C using trichlorobenzene as a solvent. Thermal properties were determined by differential scanning calorimetry (DSC-2910, TA instruments) at 10°C/min heating and cooling rates. Thermal stability of TBBPA was evaluated by thermogravimetric analysis (TGA-2950, TA instruments) at 10°C/min heating rate (Fig. 1). Other properties were obtained from the literature and listed in Table I.

Sample preparation

The blends of iPP with TBBPA ranging in volume fractions from 0 to 0.2 were prepared by premixing iPP pellets with TBBPA powders in desired proportions followed by melt blending using a single screw extruder (Brabender, 25 : 1 L/D $^3/_4''$ Independent Extruder) at temperatures of 200 - 220°C. Extrudate was quenched using cooling water bath and subsequently dried at 80°C overnight. Dried samples were chopped and molded with compression molding machines. One of the compression molding machines was maintained at 220°C for melting and the other one was maintained at 40°C for cooling,

TABLE I
Material Properties

Properties	Unit	iPP	TBBPA
Molar mass	g / mol	49,000 (Mn); 354,000 (Mw)	544
Degree of polymerization	–	1,164	N/A
Molar volume	cm^3 / mol	48.06[a] (propylene unit)	257
Density	g / cm^3	0.905	2.12
Heat of fusion	J / mol	3,900 (propylene unit)	32,600
Melting temperature	K (°C)	439 (166)	460 (187)
Crystallization temperature	K (°C)	382 (109)	N/A
Solubility parameter	$MPa^{1/2}$	17.2[a]	20.2[b]

[a] Typical value from Refs. 15 and 16.
[b] Estimated value from Ref. 17.

both of which were operated at about 10 MPa. Tensile test specimens were cut from a 1-mm thick plaque and fracture toughness test samples were cut from a 6-mm thick plaque. Dog-bone-shaped tensile specimens were prepared according to ASTM D638-02a, Type V specification. Fracture toughness test bars ($76 \times 12 \times 6$ mm^3) were prepared according to ASTM D5045-99. Notches were made using disc-saw (about 3-mm deep) followed by sharp razor cut under liquid nitrogen (about 2-mm deep).

Thermal analysis

Differential scanning calorimetry (DSC-2910, TA instruments) was used to measure the melting temperatures and crystallization temperatures of the samples. Each sample was sealed in a hermetic aluminum DSC pan, heated from 25°C to 200°C at 10°C/min rate and held at 200°C for equilibrium, and then cooled to 25°C at 10°C/min rate to measure crystallization temperature. This procedure was repeated to obtain reheating peak, which was used to find melting temperature. The peak maximum was taken as melting temperature and crystallization temperature.

Glass transition temperature (T_g) was measured by dynamic mechanical analysis (DMA-2980, TA instruments) which was performed for testing bars $25 \times 10 \times 3$ mm^3 in size in the three-point bending mode at 1 Hz as the temperature increased from −150°C to 100°C at 3°C/min rate. The storage modulus and loss factor (tan δ) were measured as a function of temperature and T_g was determined at which the peak value of tan δ occurred.

Mechanical characterization

Tensile properties of the samples were studied at room temperature using Instron 4200 machine. The tests were performed according to ASTM D 638-02a using Type V specimens at 10 mm/min cross-head speed. Fracture toughness properties were studied at room temperature according to ASTM D 5045-96 using single-edge notched bend (SENB) specimens at 50 mm/min cross-head speed. All the samples were conditioned at room temperature overnight before testing. At least five specimens were tested and the results were calculated as averages.

X-ray scattering

Crystal structure was examined by wide-angle X-ray scattering (WAXS, Molecular Methology M2) operated with Cu-Kα radiation using 1-mm thick plaque specimens.

Optical microscopy

Phase separation process was visually observed using an optical microscope (Olympus BX51) equipped with a hot stage (Linkam TMS-93) and a temperature controller (Linkam THMS-600). Each sample was put between a pair of microscope glasses and heated from 25°C to 200°C at 10°C/min rate and held at 200°C for 1 minute, and then cooled to 25°C at 10°C / min. Dispersion of TBBPA particles was observed by both optical microscopy and confocal microscopy (Leica TCS SP2). A sample was obtained from a four-point bend double crack specimen as suggested by Sue et al.[18] Core portion of the incomplete crack was cut and cryo-microtomed (Leica Ultracut) at −120°C so that the dispersion of the particles as well as the morphology along the crack propagation path can be analyzed.

Scanning electron microscopy

The morphology of each sample was examined by field-emission scanning electron microscopy (JEOL FX-6210) with an accelerating voltage of 5–10 kV. Undeformed samples were prepared by splitting 1-mm thick plaque specimens under liquid nitrogen on top of a sharp razor blade to examine the morphology of TBBPA particles. Deformed samples were prepared by cryo-cutting of the tensile specimens after

the tension test along the direction of deformation to investigate the morphology around TBBPA particles under tension. Fractured surface was investigated using the broken piece of SENB specimens after three-point bending test. The exposed cross-section was coated with Au using sputter coating machine (Cressington Sputter Coater 108). The four-point bend double crack specimen was also investigated with scanning electron micorscopy (SEM).

Viscometry

The steady state shear viscosity of the samples was measured using a parallel plate rheometer (AR-2000, TA instruments) at 180°C and 200°C. Each sample was placed between the parallel disc plates (gap, 0.8 mm) and heated until the temperature was equilibrated at the target value. Once thermal equilibrium was reached, shear viscosity was measured at constant temperature as a function of shear rate (0.001–1 s^{-1}). Since the shear viscosity decreased slightly as shear rate increased, the viscosity at a shear rate of 0.01 s^{-1} was chosen as the low shear viscosity to evaluate the processability.

RESULTS AND DISCUSSION

Thermally induced phase separation (TIPS)

The phase separation process of the mixtures of iPP and TBBPA upon cooling is investigated by optical microscopy (Fig. 2). Equilibrium phase diagram is calculated based on Flory-Huggins solution thermodynamics[19] and shows good agreement with the

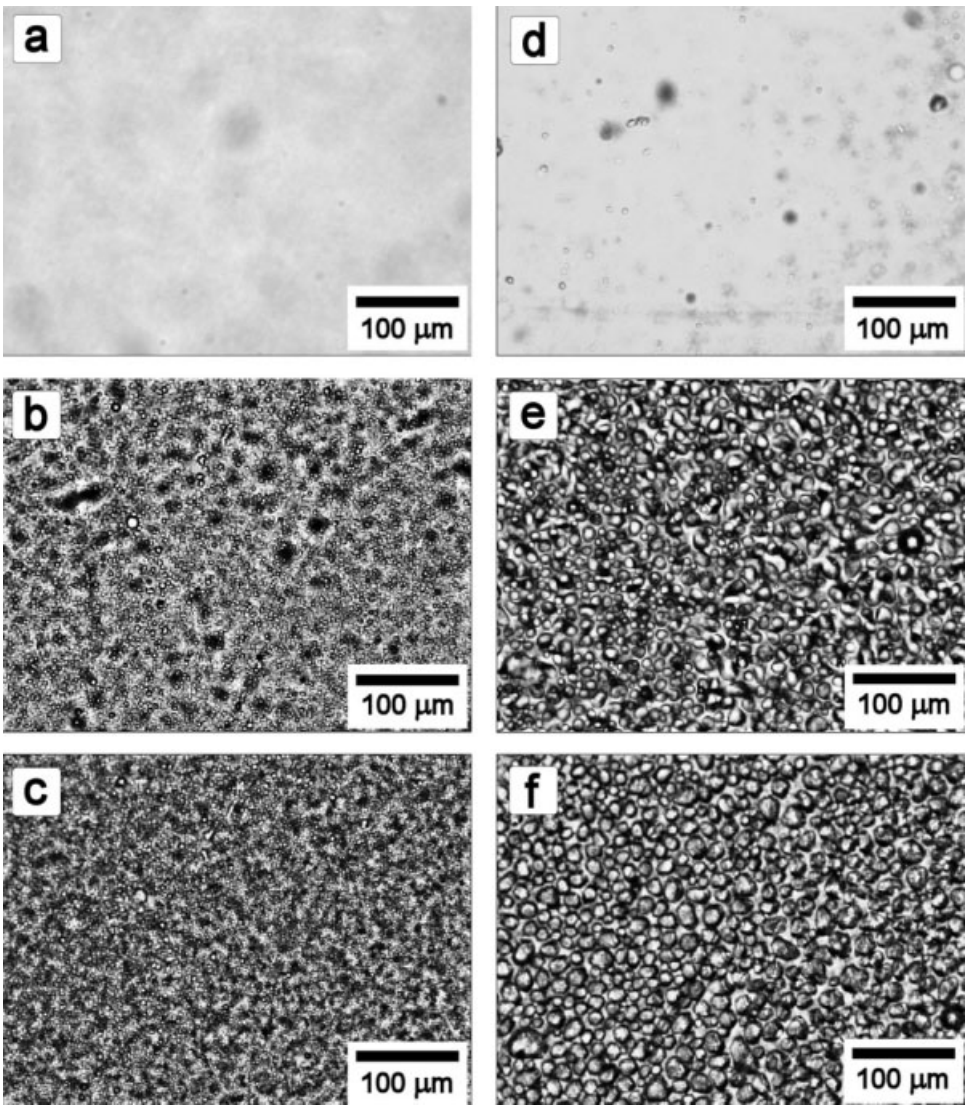

Figure 2 Photomicrographs taken by 45° polarized optical microscopy while mixtures of TBBPA and iPP were cooled from 200°C at 10°C/min rate (scale bar is 100 μm). (a) iPP/TBBPA = 9/1 (v/v) at 200°C, (b) iPP/TBBPA = 9/1 (v/v) at 160°C, (c) iPP/TBBPA = 9/1 (v/v) at 140°C, (d) iPP/TBBPA = 8/2 (v/v) at 200°C, (e) iPP/TBBPA = 8/2 (v/v) at 170°C, (f) iPP/TBBPA = 8/2 (v/v) at 140°C.

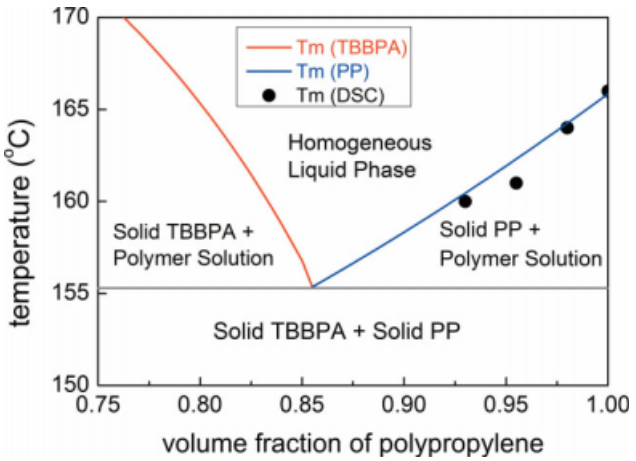

Figure 3 Equilibrium phase diagram for a mixture of TBBPA and iPP (liquidus lines are calculated results and circles are melting temperatures measured by DSC at 10°C/min heating rate). [Color figure can be viewed in the online issue, which is available at www.interscience.wiley.com.]

experimental results obtained from DSC as shown in Figures 3 and 4. Theoretical melting temperature of iPP in which a crystalline iPP is in equilibrium with a polymer solution can be calculated using eq. (1).

$$\frac{1}{T_m} = \left[1 + \frac{R\beta}{\Delta H_u}\left(\frac{V_u}{V_1}\right)(1-\phi_2)^2\right]^{-1}\left[\frac{1}{T_m^0} + \frac{R}{\Delta H_u}\left(\frac{V_u}{V_1}\right)\left\{\left(1-\frac{1}{N}\right)(1-\phi_2) - \frac{\ln(\phi_2)}{N}\right\}\right] \quad (1)$$

where T_m is the melting temperature of iPP in a polymer solution, T_m^0 is the melting temperature of neat iPP, ΔH_u is the enthalpy of fusion per repeat unit of iPP, N is degree of polymerization, ϕ_2 is the volume fraction of iPP, R is the gas constant, and β is a constant which is calculated from the solubility parameters of iPP (δ_2) and TBBPA (δ_1) along with the molar volume of TBBPA (V_1), using the equation $(\delta_1 - \delta_2)^2 V_1/R$. Five propylene units are considered as a repeat unit so that the molar volume of iPP repeat unit (V_u) and that of TBBPA (V_1) are similar to each other, as assumed in Flory-Huggins theory. Similarly, the melting temperature of TBBPA in which the crystalline TBBPA is in equilibrium with the polymer solution can be calculated using eq. (2).

$$\frac{1}{T_{m,1}} = \left[1 + \frac{R\beta\phi_2^2}{\Delta H_1}\right]^{-1}\left[\frac{1}{T_{m,1}^0} - \frac{R}{\Delta H_1}\left\{\left(1-\frac{1}{N}\right)\phi_2 + \ln(1-\phi_2)\right\}\right] \quad (2)$$

where $T_{m,1}$ is the melting temperature of crystalline TBBPA in a polymer solution, $T_{m,1}^0$ is the melting temperature of neat TBBPA, ΔH_1 is the enthalpy of fusion for neat TBBPA. According to our calculation, liquid-liquid demixing is expected to occur only when the volume fraction of iPP is less than 0.2. Within the composition range of our interest in which the volume fraction of iPP is greater than 0.8, phase separation is expected to occur by the solidification of either TBBPA or iPP, provided that the thermal transition is slow enough to maintain thermodynamic equilibrium. More detailed information about the theoretical calculation of phase diagram can be found in the literature.[20]

iPP mixed with 10 vol % of TBBPA at 200°C forms a homogeneous mixture as shown in Figure 2(a). This mixture undergoes phase separation upon cooling and TBBPA-rich droplet phase begins to grow in the iPP-rich matrix phase when the temperature reaches about 160°C [Fig. 2(b)]. These droplets keep growing until the whole sample solidifies at approximately 140°C [Fig. 2(c)]. As the temperature decreases, the mixture becomes more turbid due to a decrease in miscibility. Similar behavior was observed for a polymer solution containing 20 vol % of TBBPA. Phase separation initiates when the temperature reaches about 170°C [Fig. 2(e)], which is higher than that for 10 vol % TBBPA mixture, and the droplets keep growing until the temperature reaches about 140°C [Fig. 2(f)]. Because of the larger amount of TBBPA and the longer time for droplet growth, the mixture containing 20 vol % of TBBPA develops larger droplets compared with that containing 10 vol % TBBPA. These observations indicate that the size of TBBPA particles strongly depends on the composition of the mixture under the same thermal processing conditions.

While a melting temperature depression is observed, which is expected for miscible mixtures, the glass transition temperature (T_g) of iPP increases

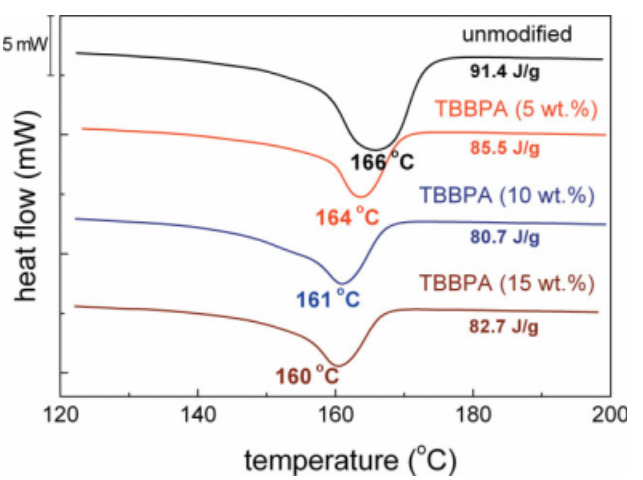

Figure 4 DSC thermograms of selected samples for melting temperature determination (reheating run at 10°C/min rate). [Color figure can be viewed in the online issue, which is available at www.interscience.wiley.com.]

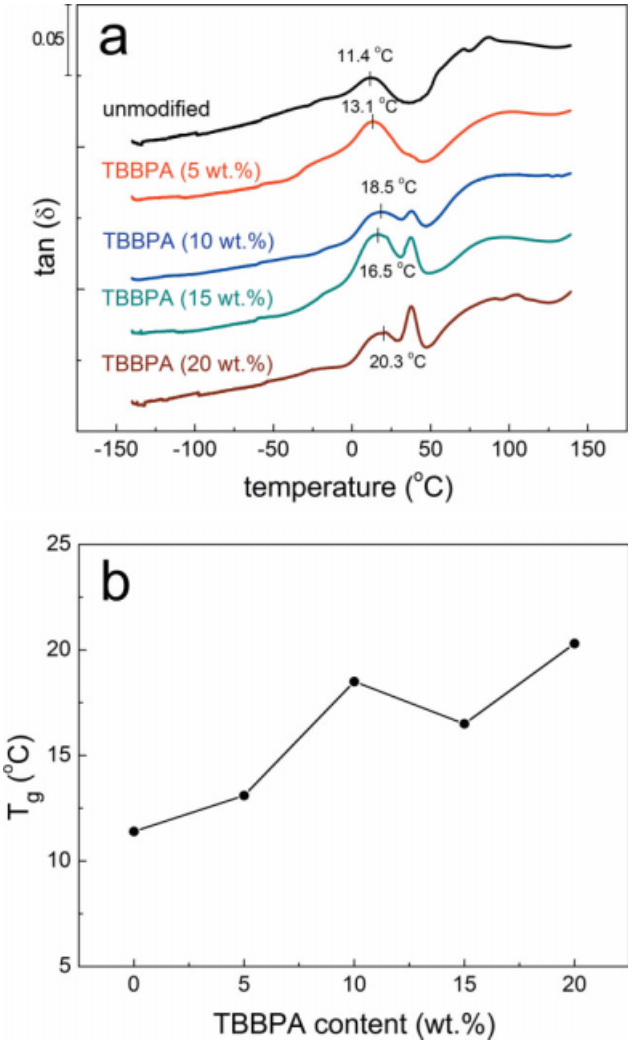

Figure 5 Dynamic mechanical analysis result measured at 1 Hz, 3°C/min heating rate. (a) Loss factor (tan δ) versus temperature and (b) T_g versus TBBPA content. [Color figure can be viewed in the online issue, which is available at www.interscience.wiley.com.]

as TBBPA content increases (Fig. 5). If TBBPA crystals act like a plasticizer, the T_g is expected to decrease, which is not the case. This indicates that TBBPA crystals do not enhance the mobility of iPP molecules. Increase in T_g might be caused by the decrease in free volume of iPP in the presence of TBBPA crystals, but further studies are needed to confirm this.

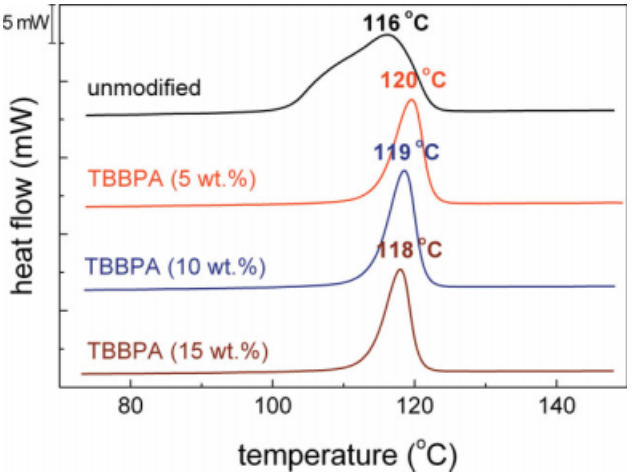

Figure 6 DSC thermograms of selected iPP/TBBPA mixtures obtained by cooling runs from 200°C at 10°C/min rate. [Color figure can be viewed in the online issue, which is available at www.interscience.wiley.com.]

Crystallization

Crystallization of the mixtures with different compositions was studied using DSC, optical microscopy and wide-angle X-ray scaterring (WAXS). Figure 6 shows DSC thermograms obtained by cooling each sample from 200°C at 10°C/min rate. With the addition of TBBPA, the width of the exothermic peak (due to crystallization) becomes much narrower and the crystallization temperature increases slightly. However, the amount of TBBPA in the range between 5 and 15 wt % does not make any appreciable difference on the crystallization of iPP. This implies that the crystallization rate of iPP increases significantly with the addition of TBBPA, but the effect of TBBPA on crystallization rate is already saturated at 5 wt % loading of TBBPA.

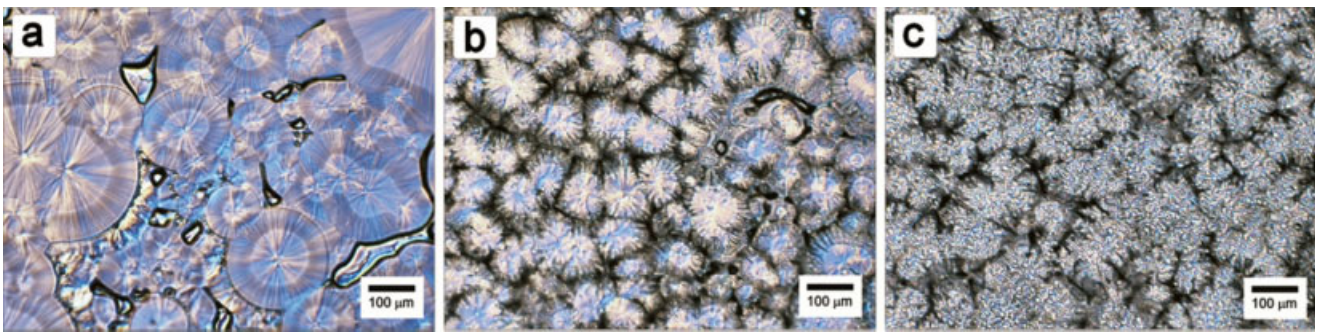

Figure 7 Micrographs of iPP spherulites taken by cross-polarized optical microscopy at room temperature. (a) Neat iPP, (b) 10 wt % TBBPA/iPP, (c) 20 wt % TBBPA/iPP. [Color figure can be viewed in the online issue, which is available at www.interscience.wiley.com.]

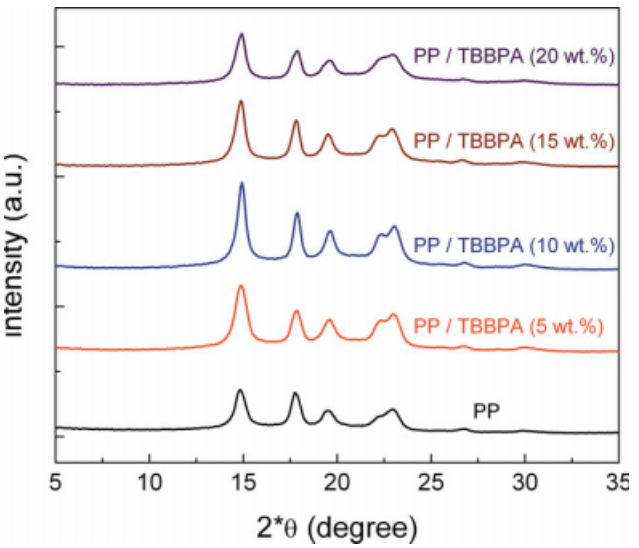

Figure 8 Wide-angle X-ray scattering results for mixtures of iPP and TBBPA. [Color figure can be viewed in the online issue, which is available at www.interscience.wiley.com.]

Spherulites of iPP were observed using cross-polarized optical microscopy. Figure 7 shows that the spherulites of iPP become smaller in size and more uniform in size distribution with the addition of TBBPA. This indicates that the diffusion of iPP molecules to the crystal growing sites becomes significantly enhanced due to the molten TBBPA which acts like a processing aid. It is also possible that TBBPA acts like a nucleating agent to enhance crystallization of iPP, but it seems less likely in this case since the increase of crystallization temperature is not as high as expected from most nucleating agents and the spherulite size does not decrease as much, either. However, the small change in size of the iPP spherulites affects the endothermic melting process as shown in Figure 4, which shows melting temperature depression due to the decreased size of iPP spherulites in the presence of TBBPA.

Although TBBPA affects the rate of crystallization noticeably, it does not affect the crystal structure of iPP. WAXS results for neat iPP show that iPP crystals are mostly in α-form. The peak positions in WAXS do not change in the presence of TBBPA, indicating that the crystal structure of iPP does not change (Fig. 8). No significant change in melting temperature also excludes the possibility of producing β-form crystals of iPP, whose typical melting temperature is about 150 °C.[21]

Viscosity

Steady state shear viscosity was measured to evaluate the effect of TBBPA on processability. Figure 9 shows that the viscosity decreases as the amount of TBBPA increases when the test temperature is above the melting temperature of the mixture, indicating that TBBPA acts like a processing aid at the test temperatures (180 °C, 200 °C). Enhanced processability by TBBPA is a great advantage over the conventional solid particle toughening in which the processing becomes difficult due to the sharp increase of melt viscosity.

Morphology of composites

Size, shape, and dispersion of TBBPA particles were examined from 1-mm thick compression-molded specimens that were conditioned at room temperature for a week before cryo-fracture (Fig. 10). Addition of 5 wt % of TBBPA to iPP produces very small particles (typical diameter is far below 1 μm) along with a few rod-like crystals. As the amount of TBBPA increases, average particle size also increases. Most of the particles bigger than 1 μm are not spherical; they are composed of anisotropic, faceted particles. This is most likely due to the unique crystal growth pattern of TBBPA in iPP matrix while the mixture is cooled. Even if the samples are quickly cooled using two compression molding machines, the resulting samples almost always show anisotropic particles. Sample with 20 wt % TBBPA shows significant amount of anisotropic particles with sharp edges, some of which are almost 10 μm in size. These particles are potentially detrimental to fracture toughness.

Tensile properties

Figure 11 shows the engineering stress–strain curve obtained from tension test at 10 mm/min cross-head speed. It can be clearly seen that the yield stress (taken as the peak stress) decreases with the increasing amount of TBBPA, which indicates dewetting of

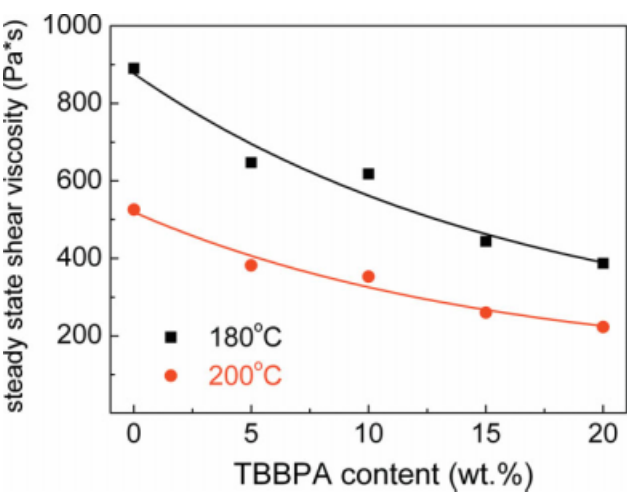

Figure 9 Steady state shear viscosity at the shear rate of 0.01 s^{-1}. [Color figure can be viewed in the online issue, which is available at www.interscience.wiley.com.]

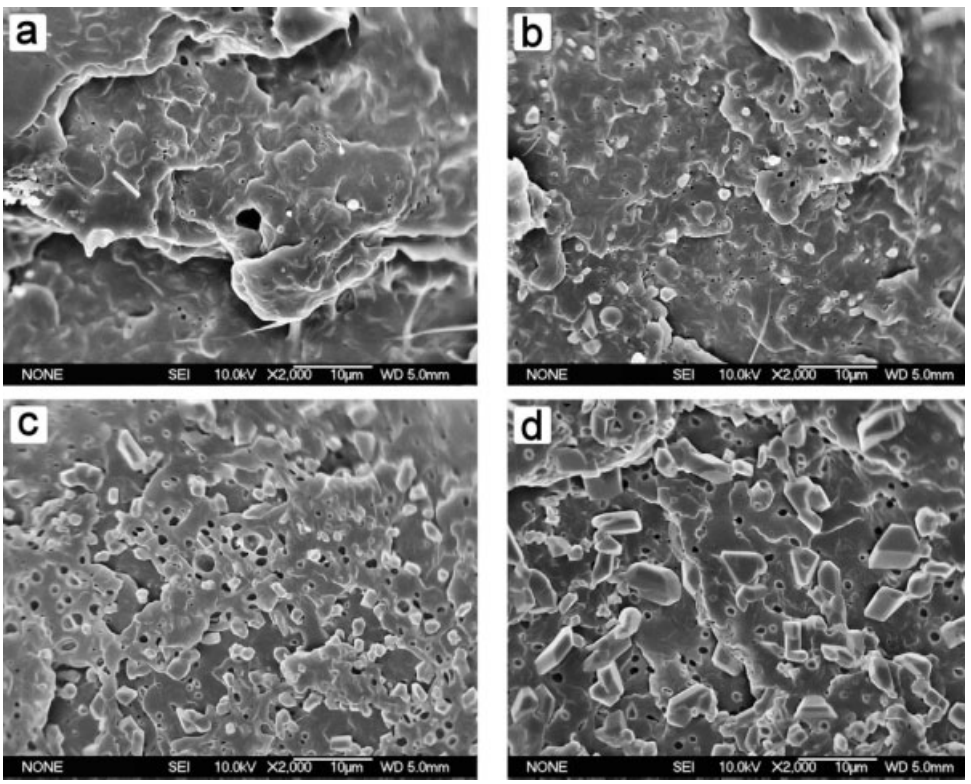

Figure 10 SEM micrographs of composite materials. (a) 5 wt % TBBPA/iPP, (b) 10 wt % TBBPA/iPP, (c) 15 wt % TBBPA/iPP, and (d) 20 wt % TBBPA/iPP.

TBBPA particles prior to the plastic deformation. Elongation at break increases as TBBPA content increases up to 15 wt %, which results in the increase of tensile toughness (as calculated from the area under the stress–strain curve). However, 20 wt % addition of TBBPA causes the elongation at break to decrease, possibly because of poor dispersion which produces oversized particles that might act as defects. Young's modulus as calculated from the initial 2% strain range does not change much. It is well known that the addition of soft particles causes significant decrease in modulus whereas rigid particles causes the modulus to increase noticeably. In this regard, TBBPA acts more like rigid particles but the expected increase in modulus is compromised by the low mechanical properties of TBBPA particle itself together with weak adhesion to polymer matrix.

The morphology around TBBPA particles clearly shows the dewetting of the particles from the polymer matrix during tensile deformation (Fig. 12). SEM micrographs were taken from the tensile specimens of iPP/TBBPA (85/15, wt/wt) after the tension test, which were sectioned along the direction of deformation to investigate the evolution of dewetting around TBBPA particles. Figure 12(a) shows the morphology around the TBBPA particles that was under tension but did not undergo necking. Dewetting of polymer matrix around the TBBPA particles can be seen (marked with arrows), which suggests weak adhesion between the two components. Overall morphology shows elliptical cavities that are stretched parallel to the direction of tension [Fig. 12(b)]. In the necking region, dewetted region of polymer matrix is further stretched to form highly elongated cavities as marked with arrows in Figure 12(c). Overall morphology of the necking region shows highly elongated cavities [Fig. 12(d)]. Dewetting and the subsequent plastic flow (void growth) around TBBPA particles induced increased elongation at break and increased tensile toughness.

Fracture toughness

The fracture toughness as measured from three-point bending test at room temperature is shown in Figure 13 and summarized in Table II. Total fracture energy (J_Q), which is the sum of energy release rate from brittle fracture response (J_{el}) and the plastic component from J-integral work of fracture ($2\int Pdx/(B(W-a))$), is calculated by eq. (3) as suggested by Landes and Begley.[22]

$$J_Q = J_{el} + \frac{2\int Pdx}{B(W-a)} = \frac{K_Q^2}{E/(1-\nu^2)} + \frac{2\int Pdx}{B(W-a)} \qquad (3)$$

where P and x are load and displacement in three-point bending test, respectively, B is the thickness,

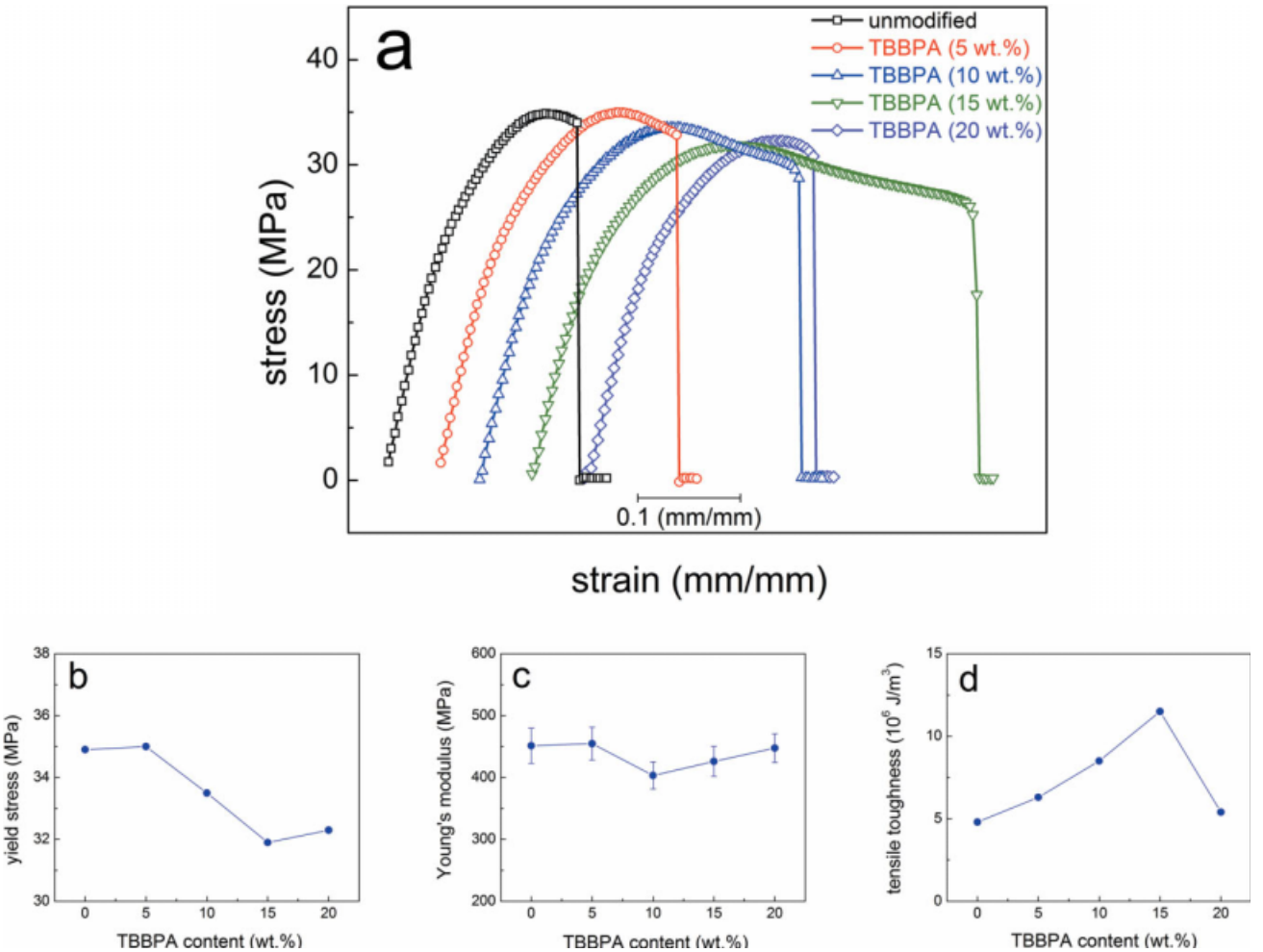

Figure 11 Tensile properties measured at room temperature. (a) Engineering stress versus strain curve (curves are shifted along the strain axis for clarity), (b) yield stress versus TBBPA content, (c) Young's modulus versus TBBPA content, with error bars, and (d) tensile toughness versus TBBPA content, as calculated from the area under the stress versus strain curve. [Color figure can be viewed in the online issue, which is available at www.interscience.wiley.com.]

W is the width, a is the pre-crack length of SENB specimen, K_Q is stress intensity factor, and E is Young's modulus. Poisson's ratio (ν) is assumed to have a typical value of 0.35. SENB specimens with 6 mm in thickness were tested at 50 mm/min crosshead speed. Stress intensity factor decreases as TBBPA content increases. This is most likely due to the large agglomerates that triggered brittle fracture during the deformation test. Total fracture energy of 10 vol % TBBPA/iPP composite is lower than that of neat iPP while further incease in TBBPA content (15–20 vol %) shows increasing trend in total fracture energy due to increase in plastic component of total fracture.

The trends in fracture toughness results do not agree with the tensile toughness results. As TBBPA content increases, tensile toughness increases mainly due to the increase in elongation at break, but fracture toughness decreases due to premature brittle failure. As discussed by Thio et al.,[8] this is not surprising since these two test methods are fundamentally different. In case of slow tensile test, the whole gauge volume responds to the applied stress. However, only the material directly in front of the notch tip, which causes very low level of plastic response, will contribute to the measured fracture toughness. The presence of sharp notch together with higher test speed result in a large increase of local strain rate in fracture toughness test, compared with the slow strain rate in tensile test.

Fractured surface after the three-point bending test was investigated by SEM (Fig. 14). Neat iPP shows featureless, clean surface indicating highly brittle fracture behavior [Fig. 14(a)]. In contrast, TBBPA-containing samples exhibit highly stretched appearance near the crack tip in which strain is highly concentrated, indicating the occurrence of dewetting followed by plastic flow [Fig. 14(b)]. However, the overall resistance to crack propagation becomes significantly lower as evident from the

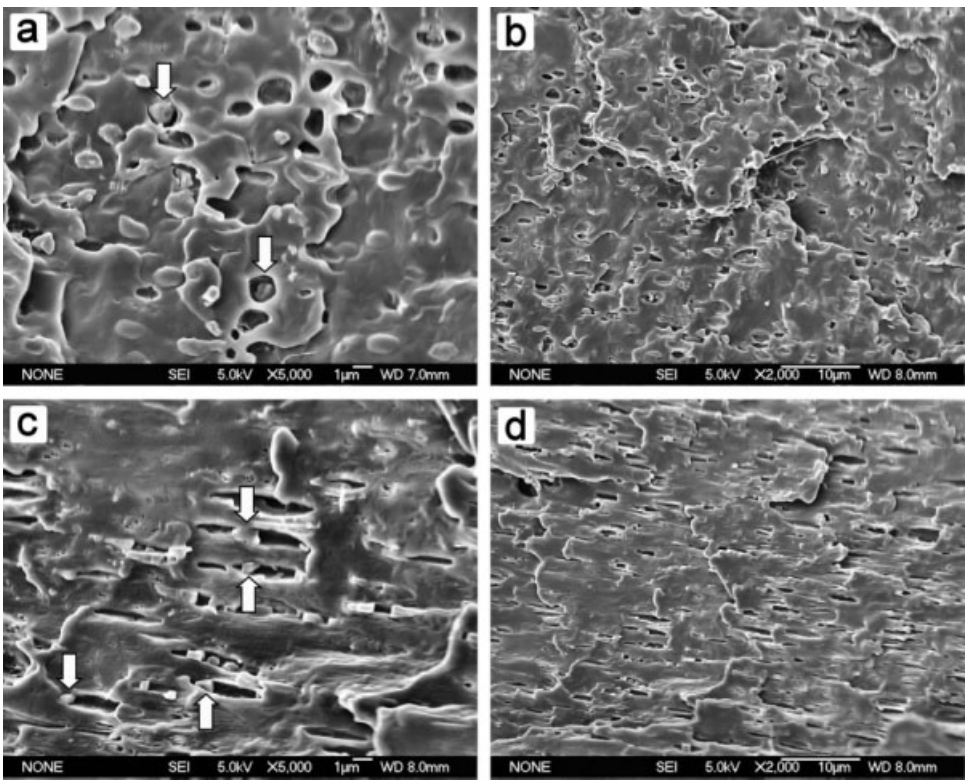

Figure 12 SEM micrographs of iPP + 15 wt % TBBPA (cross-sections are obtained by cryo-cutting of the tensile specimens after the tension test along the direction of deformation). (a) Outside of necking region at high magnification, (b) outside of necking region at low magnification, (c) necking region at high magnification, and (d) necking region at low magnification.

noticeably decreased peak load with the addition of TBBPA, possibly due to the premature failure caused by oversized TBBPA particles (Fig. 13). Because the crack propagates through the path with least resistance, only the weakest material points in front of the crack would contribute to the total fracture energy. If the propagating crack encounters oversized TBBPA particles, flaw-induced brittle fracture would result without any appreciable resistance from the polymer matrix. It seems that initially promising response (dewetting followed by plastic flow) could not be maintained due to the large flaws caused by slow cooling of thick specimens and poor dispersion of TBBPA particles. Highly stretched morphology is observed only near the crack-tip region; fractured surface becomes smooth as the distance from the crack tip increases [Fig. 14(c)].

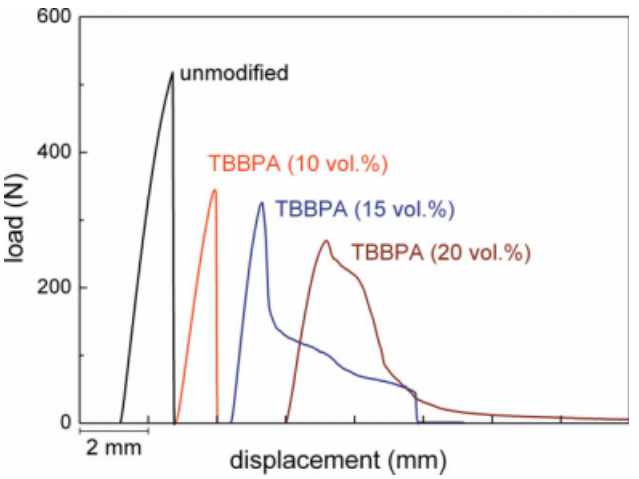

Figure 13 Load versus displacement curve from the three-point bending test for single-edge notched bend specimens performed at room temperature with cross-head speed of 50 mm/min (curves are shifted along the displacement axis for clarity). [Color figure can be viewed in the online issue, which is available at www.interscience.wiley.com.]

Several authors argued that the surface-to-surface interparticle distance, which is determined by the volume fraction of the particle and the size of the particle, is a key factor that governs the fracture

TABLE II
Fracture Toughness Calculated from Three- Point Bending Test at 50 mm/min Cross-Head Speed

TBBPA (vol %)	K_Q (MPa*m$^{1/2}$)	J_{el} (kJ/m^2)	$2\int Pdx/B(W-a)$ (kJ/m^2)	J_Q (kJ/m^2)
0	2.13	10.2	13.0	23.2
10	2.14	10.3	7.6	17.9
15	1.64	6.0	17.6	23.6
20	1.27	3.6	22.2	25.8

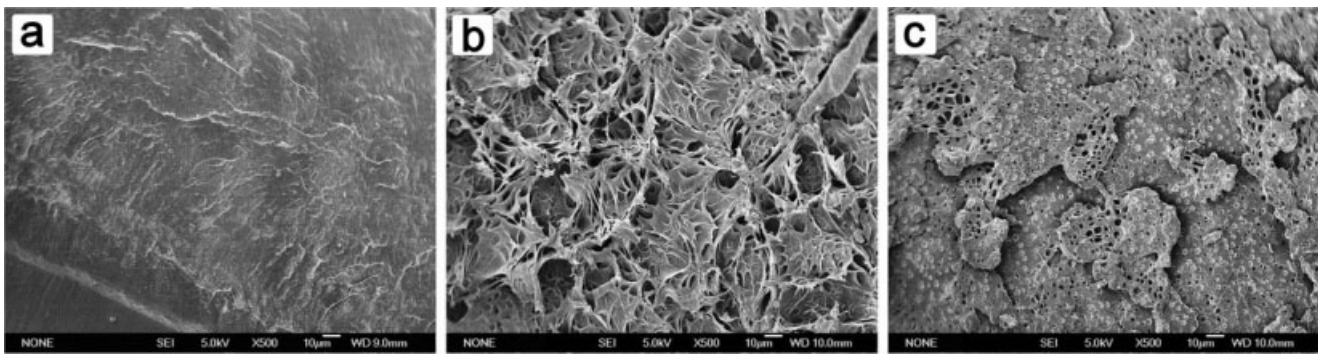

Figure 14 SEM micrographs of the fractured surface after the three-point bending test. (a) Neat iPP, near crack tip region; (b) TBBPA 10 vol %, near the crack tip region; and (c) TBBPA 10 vol %, far-away region from the crack tip. Scale bar is 10 μm.

behavior.[6–12] According to this argument, crystallization of semicrystalline polymers is initiated from the incoherent polymer-particle interface and forms low energy planes of oriented crystals in the near-interface layer of the polymer with specific thickness. If the thickness of this oriented crystalline layer between particles is below a certain critical value (critical ligament thickness, which depends on the polymer matrix), easily stretchable ligaments with reduced plastic resistance will percolate throughout the structure which promotes plastic response of the entire material. If the surface-to-surface distance is above the critical ligament thickness, oriented layers of reduced plastic resistance around particles do not percolate through the structure and the overall plastic resistance is substantially elevated which will cause the fracture behavior to be governed by the extrinsic flaws that leads to premature brittle fracture. If these arguments are applied to our case, the fundamental requirement would be that TBBPA should crystallize first so that iPP crystals can grow from the surface of these TBBPA particles and form low energy crystal planes to facilitate plastic deformation. In this regard, the crystallization of neat TBBPA was investigated by DSC. In the first heating run in DSC, an endothermic melting peak appears at 187°C, but no exothermic crystallization peak is observed in the subsequent cooling run [Fig. 15(a)]. At the end of this first cycle, TBBPA is likely in its super-cooled state. In the second heating run, an exothermic (crystallization) peak appears at 71°C, followed by a melting peak at 167°C [Fig. 15(b)]. It seems that the mobility of the super-cooled TBBPA increases enough at 71°C so that the rearrangement of the unstable state TBBPA takes place, which leads to crystallization of TBBPA. Those crystals melt at 167°C. However, there is no exothermic (crystallization) peak in the subsequent cooling, even if the cooling rate is decreased from 10°C/min to 5°C/min. Third cycle performed at 5°C/min rate shows the same behavior as the second cycle (result not shown). This indicates that the crystallization of neat TBBPA is very slow and cannot happen at 5 – 10°C/min cooling rate. Because the actual samples were prepared at much higher cooling rate, it is likely that iPP crystallizes first while TBBPA is still in super-cooled liquid state during cooling process.

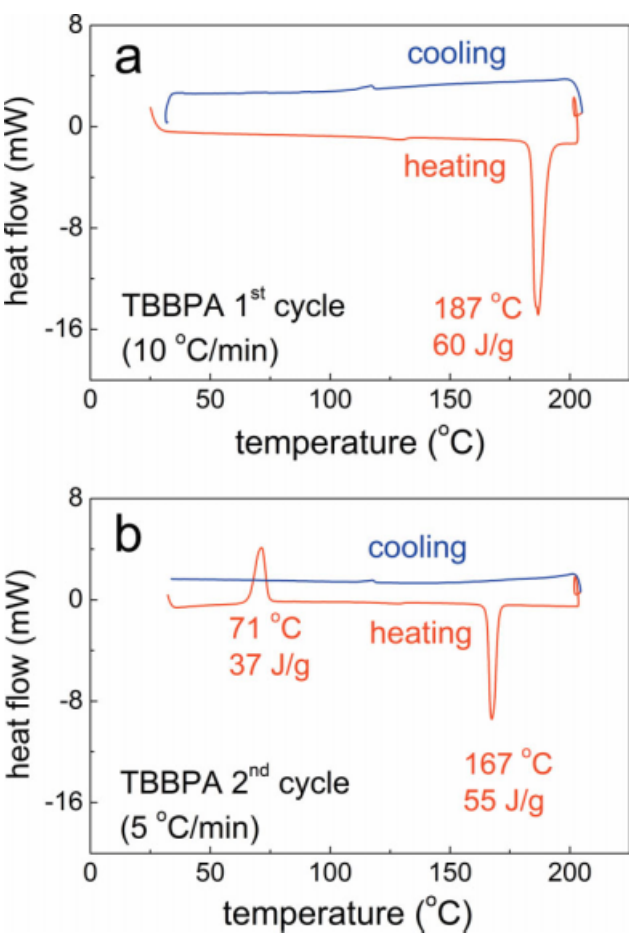

Figure 15 DSC thermograms of neat TBBPA. (a) First cycle of heating and cooling at 10°C/min rate and (b) second cycle of heating and cooling at 5°C/min rate. [Color figure can be viewed in the online issue, which is available at www.interscience.wiley.com.]

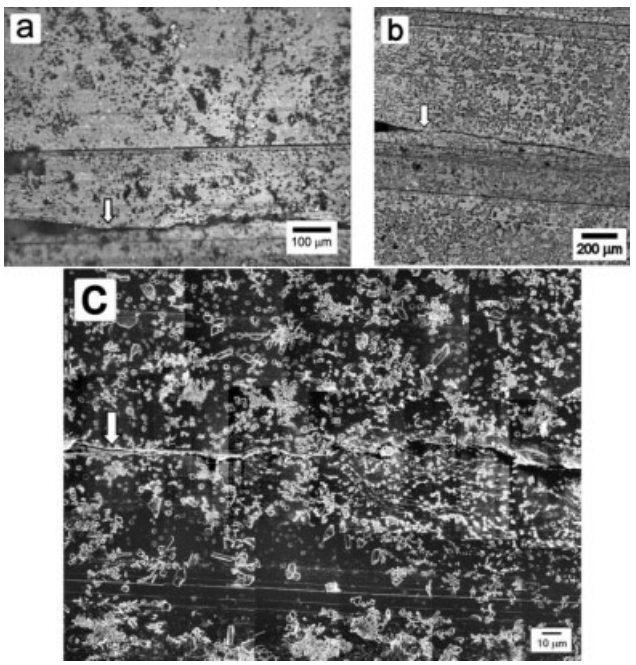

Figure 16 Morphology along the crack propagation path (crack tip region is indicated with an arrow). (a) Optical microscopy, (b) confocal microscopy, and (c) SEM.

Since the super-cooled TBBPA is unstable, it would gradually crystallize to form large crystals during the conditioning step at room temperature (which is above the T_g of iPP) as shown in Figure 10.

The morphology along the crack propagation path was investigated for an iPP compound containing 15 vol % TBBPA using optical microscopy, confocal microscopy, and SEM. The sample was taken from the core section of the incompletely broken crack of the four-point double crack specimen after fracture, followed by cryo-microtoming. Stress-whitening zone is not observed by optical microscopy, indicating that the plastic resistance near the crack tip is not significant [Fig. 16(a)]. Substantial amount of large agglomerates of TBBPA particles in the micrograph clearly shows poor dispersion. Similar morphology is observed by confocal microscopy [Fig. 16(b)]. It can be seen that the crack propagates nearly straightly, indicating there is no appreciable toughening effect by crack deflection mechanism, either. SEM micrograph shows that the particles not only aggregate to form large agglomerates, but also the particles have anisotropic, sharp-edged shapes [Fig. 16(c)]. It is generally accepted that the particles with sharp edges are more likely to induce brittle fracture and should be avoided to prevent premature brittle fracture. However, it is not possible to prevent these anisotropic crystals under the current experimental conditions. Preparation of 6-mm thick specimens for fracture toughness to ensure plane strain condition inevitably result in relatively slow cooling in the core section of the specimens in which large anisotropic crystals of TBBPA can easily form. Dependence of particle geometry on thermal treatment is currently one drawback of this strategy.

CONCLUSION

Organic crystalline compound (tetrabromobisphenol-A) was tested as a toughening agent for isotactic polypropylene (iPP), which forms a homogeneous mixture at high temperature and acts as a processing aid, but undergoes phase separation upon cooling to form crystalline particles and acts as a toughening agent. Viscosity decreased as tetrabromobisphenol-A (TBBPA) content increased at high temperature, indicating enhanced processability. The reduced viscosity facilitated the diffusion of iPP during crystallization and accelerated the crystallization of iPP significantly as a result. Increase in crystallization rate is beneficial to increase productivity in most polymer processing applications. Addition of TBBPA caused decrease in tensile yield stress, increase in elongation at break and tensile toughness and negligible change in Young's modulus. This indicates that the interfacial adhesion between TBBPA particle and iPP matrix is weak and dewetting of TBBPA particle occurs at the early stage of deformation as a consequence, which was confirmed from the morphology of deformed region by SEM. The fracture toughness as measured by three-point bending test, however, decreased as TBBPA content increased. This is most likely due to the poorly dispersed, oversized particles. Micrographs taken along the crack propagation path showed large agglomerates of TBBPA particles with sharp edges, which can easily trigger premature brittle failure.

It was also found that the crystallization of TBBPA is very slow and cannot form small crystals quickly under our cooling condition. Because of the slow crystallization of TBBPA, it is not clear whether iPP crystals can grow from the surface of TBBPA to form low energy crystal layers that should provide easy plastic deformation, as other investigators observed with rigid inorganic particles[7,8,11,12] and soft rubber particles.[6,9,10] In this regard, efficient organic crystalline compound for toughening is supposed to form small crystals very quickly prior to polymer crystallization.

References

1. Bucknall, C. B.Toughened Plastics; Applied Science Publishers: London, 1977.
2. Kinloch, A. J.; Young, R. J.Fracture Behavior of Polymers; Applied Science Publishers: London, New York, 1983.
3. Liang, J. Z.; Li, R. K. Y. J Appl Polym Sci 2000, 77, 409.
4. Lazzeri, A.; Bucknall, C. B. J Mater Sci 1993, 28, 6799.
5. Lazzeri, A.; Bucknall, C. B. Polymer 1995, 36, 2895.
6. Wu, S. J Appl Polym Sci 1988, 35, 549.

7. Bartczak, Z.; Argon, A. S.; Cohen, R. E.; Weinberg, M. Polymer 1999, 40, 2347.
8. Thio, Y. S.; Argon, A. S.; Cohen, R. E.; Weinberg, M. Polymer 2002, 43, 3661.
9. Muratoglu, O. K.; Argon, A. S.; Cohen, R. E.; Weinberg, M. Polymer 1995, 36, 921.
10. Bartczak, Z.; Argon, A. S.; Cohen, R. E.; Weinberg, M. Polymer 1999, 40, 2331.
11. Bartczak, Z.; Argon, A. S.; Cohen, R. E.; Kowalewski, T. Polymer 1999, 40, 2367.
12. Wilbrink, M. W. L.; Argon, A. S.; Cohen, R. E.; Weinberg, M. Polymer 2001, 42, 10155.
13. Lesser, A. J.; McCarthy, T. J.; Yoon, J.; Yordem, O. S.USPTO. Pat. Pending, USSN 12/057850 (2008).
14. Yoon, J.; McCarthy, T. J.; Lesser, A. J. SPE Antec 2008, 6.
15. Brandrup, J.; Immergut, E. H.; Grulke, E. A.Polymer Handbook; Wiley: New York, 1999.
16. Barton, A. F. M. CRC Handbook of Solubility Parameters and Other Cohesion Parameters; CRC Press: Boca Raton, 1991.
17. Hansen, C. M. Prog Org Coat 2004, 51, 109.
18. Sue, H. J.; Pearson, R. A.; Parker, D. S.; Huang, J.; Yee, A. F. Polym Prep (Am Chem Soc Div Pokym Chem) 1998, 29, 147.
19. Flory, P. J.Principles of Polymer Chemistry; Cornell University Press: Ithaca, NY, 1953.
20. Burghardt, W. R. Macromolecules 1989, 22, 2482.
21. Zhao, S.; Cai, Z.; Xin, Z. Polymer 2008, 49, 2745.
22. Landes, J. D.; Begley, J. A. ASTM STP 6321977.